Measurement-induced dynamics of many-body systems at quantum criticality

Davide Rossini and Ettore Vicari
Dipartimento di Fisica dell'Università di Pisa and INFN, Largo Pontecorvo 3, I-56127 Pisa, Italy

(Received 4 February 2020; revised 24 June 2020; accepted 24 June 2020; published 9 July 2020)

We consider a dynamic protocol for quantum many-body systems, which enables us to study the interplay between unitary Hamiltonian driving and random local projective measurements. While the unitary dynamics tends to increase entanglement, local measurements tend to disentangle, thus favoring decoherence. The competition of the two drivings is analyzed at quantum transitions, where the presence of critical correlations substantially changes the impact of local measurements. We identify a particular regime (dynamic scaling limit) within a dynamic scaling framework, where the two mechanisms develop a nontrivial interplay and peculiar scaling behaviors. This is supported by a numerical analysis of a measurement-driven quantum Ising chain. The local measurement process generally tends to suppress quantum correlations, even in the dynamic scaling limit. The power law of the decay of the quantum correlations turns out to be enhanced at the quantum transition.

DOI: 10.1103/PhysRevB.102.035119

I. INTRODUCTION

One of the greatest challenges of modern statistical mechanics is understanding and controlling the quantum many-body dynamics. The recent progress in atomic physics and quantum optical technologies offers a great opportunity for thorough investigations of the interplay between the coherent quantum dynamics and the interaction with the environment, from both experimental and theoretical viewpoints [1–6]. The competition of such mechanisms may originate a subtle interplay, likely representing the most intricate dynamic regime of quantum systems where complex many-body phenomena appear. In this respect, it is worth focusing near quantum phase transitions, where quantum critical fluctuations emerge and correlations develop a diverging length scale [7,8].

In general, while the unitary evolution enhances the entanglement, measurements of observables disentangle degrees of freedom and thus tend to decrease quantum correlations, similarly to decoherence. A quantum measurement is physically realized when the interaction with a macroscopic classical object makes a quantum mechanical system rapidly collapse into an eigenstate of a specific operator, and the resulting time evolution appears to be a nonunitary projection. Such process is referred to as a projective measurement [9,10]. When the system is projected into an eigenstate of a local operator, the corresponding local degree of freedom is disentangled from the rest of the system. Moreover, if measurements are performed frequently, the quantum state gets localized in the Hilbert space near a trivial product state, leading to the quantum Zeno effect [11,12]. In strongly correlated systems, quantum phase transitions give rise to a peculiar dynamic regime where long-range correlations set in; the impact of projective quantum measurements on the decay rate of quantum correlations might be thus substantially affected by the emerging critical dynamics.

Inspired by recent pioneering studies of the entanglement dynamics in measurement-induced random unitary quantum circuits [13–15], we introduce a framework to address the interplay of unitary and projective dynamics in experimentally viable many-body systems at quantum transitions, such as quantum spin networks. For this purpose, we consider dynamic problems arising from protocols combining the unitary Hamiltonian and local measurement drivings (for a cartoon, see Fig. 1). In such conditions, it is not clear how the presence of projective measurements modifies the quantum critical behavior of a purely unitary system. One can easily imagine that different regimes emerge, depending on the measurement protocols and their parameters. If every site were measured

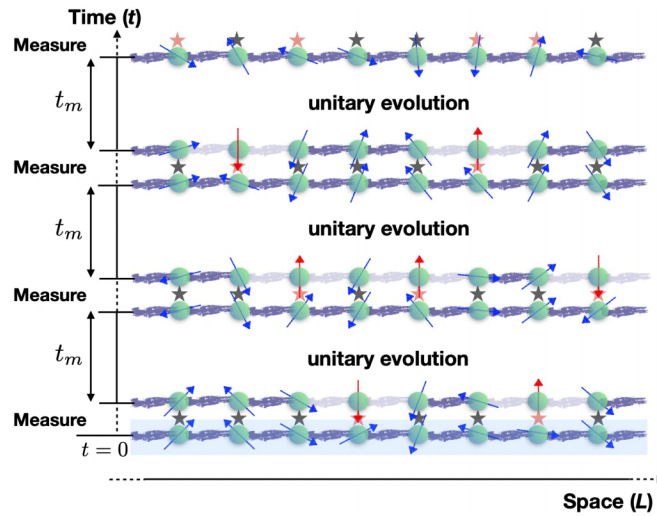

FIG. 1. Sketch of the protocol: A quantum spin system, initially frozen in its ground state at quantum criticality ($t = 0$), is perturbed with local projective measurements (stars) occurring after every time interval t_m, with a homogeneous probability p per site. In between two measurement steps, the system evolves unitarily according to its Hamiltonian. Red stars denote the occurrence of a measurement on a given site (for the sake of clarity, in the figure we considered $\sigma^{(3)}$-type measures: spins colored in red are projected along the z axis).

during each projective step, the system would be continually reset to a tensor product state. More intriguing scenarios should hold when local measurements are spatially dilute.

Most of the work done in this context focused on the investigation of entanglement transitions genuinely driven by local measurements, either in random circuits [13–22], or in the Bose-Hubbard model [23,24], on nonanaliticities emerging in quantum spin systems [25], and on measurement-induced state preparation [26]. In noninteracting models, continuous local measurements were shown to largely suppress entanglement [27]. Here we study a substantially different dynamic problem: understanding and predicting the effects of local random measurements on the quantum critical dynamics of many-body systems, i.e., when a quantum transition is driven by the Hamiltonian parameters.

II. MEASUREMENT PROTOCOLS

We consider quantum lattice spin systems, assuming that only one relevant parameter μ of the Hamiltonian $H(\mu)$ [with corresponding renormalization-group (RG) dimension $y_\mu > 0$] can deviate from the critical point located at $\mu_c = 0$. The system is initialized, at $t = 0$, in the ground state close to criticality; thus $|\mu| \ll 1$. Random local measurements are then performed at every time interval t_m, such that each site has a (homogeneous) probability p to be measured. In between two measurement steps, the system evolves according to the unitary operator $e^{-iH(\mu)t}$, where we fix $\hbar = 1$ (see Fig. 1). If $p \to 1$, each spin gets measured every t_m, and the effects of projections are expected to dominate over those of the unitary evolution. In contrast, for p sufficiently small, the time evolution may end up being unaffected by measurements. In between these two regimes, we unveil the existence of a competing unitary vs projective dynamics, characterized by controllable dynamic scaling behaviors associated with the universality class of the quantum transition.

More complex protocols may be devised. For example, the initial ground state might be replaced with a finite-temperature Gibbs state. One may also consider a quench of the control parameter at $t = 0$, starting from the ground state for a given value $\mu_0 \ll 1$, to a different value μ characterizing the unitary evolution between the measurement steps. In this case, the out-of-equilibrium evolution arises from both the initial quench and the measurement protocol. In our presentation below, we focus on the simpler version discussed before, although an extension to such more complex scenarios is possible (see Appendix A).

As for the model, we consider the paradigmatic d-dimensional quantum Ising Hamiltonian,

$$H_{\rm Is} = -J \sum_{\langle x,y\rangle} \sigma_x^{(3)} \sigma_y^{(3)} - g \sum_x \sigma_x^{(1)} - h \sum_x \sigma_x^{(3)}, \quad (1)$$

where $\boldsymbol{\sigma} \equiv (\sigma^{(1)}, \sigma^{(2)}, \sigma^{(3)})$ are spin-1/2 Pauli matrices, the first sum is over the bonds connecting nearest-neighbor sites $\langle \boldsymbol{x}, \boldsymbol{y}\rangle$, while the other sums are over the sites. We fix $J = 1$ as the energy scale. At $g = g_c$ and $h = 0$, the model undergoes a continuous quantum transition belonging to the two-dimensional Ising universality class, separating a disordered phase ($g > g_c$) from an ordered ($g < g_c$) one [7,8]. Such transition is characterized by a diverging length scale ξ of

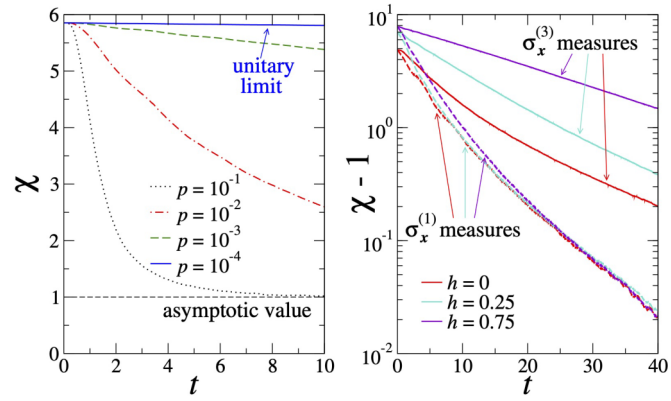

FIG. 2. Evolution of the susceptibility χ for the Ising chain with $L = 10$ and $g = 1$. Local measurements are performed along either the longitudinal [$\sigma_x^{(3)}$, continuous curves] or the transverse direction [$\sigma_x^{(1)}$, dashed curves], with $t_m = 0.1$. In the left panel we fix $h = 0$ and vary p; in the right panel we fix $p = 10^{-2}$ and vary h (see legends). Here and in the next figures data are averaged over many [$O(10^4)$] trajectories and errors are on the order of the size of the lines.

critical correlations and the suppression of the energy gap Δ as $\Delta \approx \xi^{-z}$, where $z = 1$ is the dynamic exponent. The power-law divergence of ξ is related to the RG dimensions of the relevant parameters $\delta \equiv g - g_c$ and h: it behaves as $\xi \sim |\delta|^{-1/y_\delta}$ at $h = 0$, and $\xi \sim |h|^{-1/y_h}$ for $\delta = 0$ [28].

In our dynamic protocol, we take a spin system of linear size L with periodic boundary conditions and perform, on each site, random measurements of the spin components $\boldsymbol{\sigma_x}$, along transverse [$\sigma_x^{(1)}$] or longitudinal [$\sigma_x^{(3)}$] directions, every time interval t_m and with probability p. We then project onto the measured value of the spin component and normalize the many-body wave function. The main features of the resulting evolution are inferred by fixed-time averages of observables, as magnetization $m(t)$ and susceptibility $\chi(t)$,

$$m(t) = \frac{1}{L^d} \sum_{\boldsymbol{x}} \langle \sigma_{\boldsymbol{x}}^{(3)} \rangle_t, \quad \chi(t) = \frac{1}{L^d} \sum_{\boldsymbol{x},\boldsymbol{y}} \langle \sigma_{\boldsymbol{x}}^{(3)} \sigma_{\boldsymbol{y}}^{(3)} \rangle_t, \quad (2)$$

averaging over trajectories ($\langle\cdot\rangle_t$ is the expectation value at time t). Since measurements generally suppress quantum correlations, $\chi(t \to \infty) \to 1$, corresponding to an uncorrelated state, we study the ratio $R_\chi(t) \equiv [\chi(t) - 1]/[\chi(t = 0) - 1]$, which goes from 1 ($t = 0$) to zero ($t \to \infty$). The timescale τ_m of the suppression of quantum correlations may be estimated from the halving time of $R_\chi(t)$. Further details on the various quantities that can be analyzed for dynamic protocols involving the quantum Ising model are provided in Appendix B.

As visible from the data in Fig. 2, obtained by numerically simulating a one-dimensional (1D) quantum Ising model, random spin measurements tend to destroy correlations in the system, which converges asymptotically in time to a fully disordered configuration ($\chi = 1$, $m = 0$). Details on the numerical computations are postponed in Appendix C. Here we observe that the timescale τ_m of such dynamical process depends on p (left panel), on the initial state, and the measurement axis (right panel). In particular, longitudinal measurements are less destructive than those along the

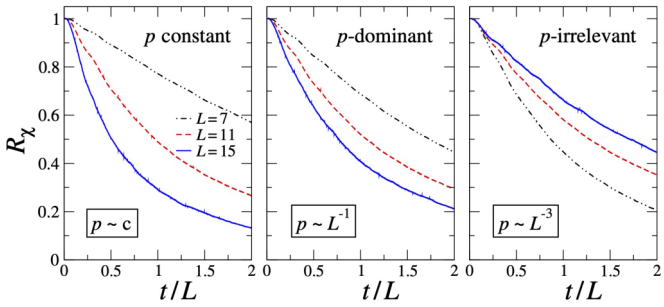

FIG. 3. Susceptibility ratio R_χ vs rescaled time tL^{-z} for the quantum critical Ising chain ($g = 1$, $h = 0$) for various L. Measurements occur along the longitudinal direction, with $t_m = 0.1$ and p either constant (left: $c = 0.005$) or equal to $p = cL^{-a}$ (middle: $a = 1$, $c = 0.05$; right: $a = 3$, $c = 5$). For $a = 0$ and $a = 1$, the timescale τ_m of quantum correlations significantly decreases with increasing L as a function of the scaling time tL^{-z}, while for $a = 3$ it clearly increases.

transverse direction, being orthogonal to the coupling and thus to the ordering direction of spins. One can gain insight on this mechanism, which resembles relaxation due to decoherence, by first looking at the exactly solvable single-spin model (see Appendix D): Irrespective of the magnetic field strength and direction, for finite t_m, the magnetization drops to zero exponentially in time, ending up into a completely unpolarized state. Deviations from pure exponentials have thus to be ascribed to the full many-body nature of the system (1).

III. DYNAMIC SCALING BEHAVIOR

To achieve a more quantitative understanding of the role of projective measurements in this context, we first focus on the quantum critical region, where universality can be helpful to control the system dynamics. Indeed, the out-of-equilibrium critical dynamics at continuous quantum transitions develops homogeneous scaling laws [30–42], even in the presence of dissipation [43,44]. One could ask whether similar scaling arguments hold in the above context. A naive application of the dynamic finite-size scaling (FSS) theory [45–47] at the critical point of the quantum Ising chain leads to the results of Fig. 3, reporting the susceptibility ratio R_χ versus the rescaled time variable t/τ, where $\tau = L^z \sim \Delta^{-1}$ is the timescale of the critical quantum correlations. If the probability p to perform measurements is kept constant while increasing the system size (left panel), the net effect of projections becomes progressively important, eventually overwhelming the unitary Hamiltonian dynamics. Therefore a putative scaling behavior could emerge only after rescaling p with L. Guided by scaling arguments, it is tempting to assume that $p \sim L^{-a}$. Figure 3 shows that while with $p \sim L^{-1}$ random measurements are still dominant (middle panel), with $p \sim L^{-3}$ they become irrelevant for the asymptotic dynamic scaling (right panel). Between these two cases, there could be a suitable power-law exponent entering the proper scaling theory for the measurement-induced dynamics described above, provided this is possible.

Taking advantage of the previous insight, we put forward a phenomenological framework in which, as a working hypothesis, we assume a scaling behavior for the parameters t_m and p characterizing the measurement procedure. We conjecture that for systems with Hamiltonian $H(\mu)$ as introduced above, a generic observable B (averaged over the trajectories) follows the scaling law

$$B(\mu, t, t_m, p) \approx b^{-y_B} \mathcal{B}(\mu b^{y_\mu}, t b^{-z}, t_m\, b^{\zeta}, p b^{\varepsilon}). \tag{3}$$

Here b denotes an arbitrary positive parameter, y_B is the critical RG dimension of the operator B, while ζ and ε are appropriate exponents associated with the measurement process, and $\mathcal{B}$ is a universal scaling function apart from normalizations (see Appendix A for more details). Equation (3) is expected to provide the power-law asymptotic behavior in the large-b limit, neglecting further dependencies on other parameters, which are supposed to be suppressed (and thus irrelevant) in such limit.

The arbitrariness of the scale parameter b in Eq. (3) can be fixed by setting $b = \lambda \equiv |\mu|^{-1/y_\mu}$, where $\lambda \sim \xi$ is the length scale of critical modes. The scaling variable associated with the time interval t_m should be given by the ratio t_m/τ, where $\tau \sim \Delta^{-1} \sim \lambda^z$ is the time scale of the critical models (this implies $\zeta = -z$). Keeping t_m fixed in the large-λ limit, the dependence on t_m disappears asymptotically, originating only $O(\lambda^{-z})$ scaling corrections. Moreover, noticing that p is effectively a probability per unit of time and space, a reasonable guess would be that its correct scaling to compete with the critical modes is $p \sim \lambda^{-z-d}$; thus,

$$\varepsilon = z + d. \tag{4}$$

This leads to the dynamic scaling equation $B(\mu, t, t_m, p) \approx \lambda^{-y_B} \mathcal{B}(t\lambda^{-z}, p\lambda^{\varepsilon})$ [48]. The value of ε in Eq. (4) is crucial, since it allows us to separate the measurement-irrelevant regime $p = o(\lambda^{-\varepsilon})$ (Fig. 3, right panel) from the measurement-dominant regime $p\lambda^{\varepsilon} \to \infty$ (Fig. 3, left and middle panels). Note that since $p \sim \lambda^{-\varepsilon}$ and $t \sim \lambda^z$, the dynamic scaling *Ansatz* predicts that the timescale τ_m associated with the suppression of quantum correlations behaves as $\tau_m \sim p^{-\kappa}$ with $\kappa = z/\varepsilon < 1$.

The above scaling theory holds in the *thermodynamic* limit $L/\lambda \to \infty$, which is expected to be well defined for any $\mu \neq 0$, for which λ is finite. Nonetheless, for most practical purposes, both experimental and numerical, one typically has to face systems of finite length. Such situations can be framed in the FSS framework, where the scale parameter in Eq. (3) is set to $b = L$ [8,39,45–47,49]. Fixing again t_m, straightforward manipulations lead to the scaling law

$$B(\mu, t, t_m, p, L) \approx L^{-y_B} \mathcal{B}(\mu L^{y_\mu}, t L^{-z}, p L^{\varepsilon}). \tag{5}$$

The proper dynamic FSS behavior is obtained for $L \to \infty$ and taking the arguments of the scaling function $\mathcal{B}$ fixed.

Analogous scaling *Ansätze* for more general observables, as fixed-time correlation functions, are obtainable with the same arguments and assumptions (see Appendix B). They can be extended to include an initial quench of the Hamiltonian parameter $\mu_0 \to \mu$ [by adding a further dependence on $\mu_0 b^{y_\mu}$ in Eq. (3)], to consider finite-temperature initial Gibbs states (by adding a dependence on $T b^{z}$), and allowing for weak dissipation [44]. Note that the scaling arguments do not depend on the type of local measurement; therefore they are expected

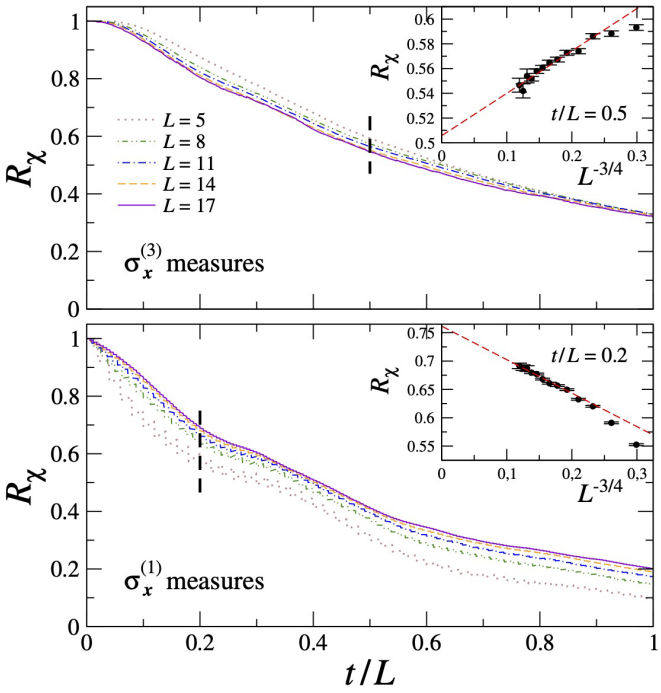

FIG. 4. Time behavior of R_χ at criticality, for various sizes. Random measurements are either along the longitudinal (upper plots) or the transverse direction (lower plots), for $t_m = 0.1$, $p = 1/L^2$ according to (4). The two insets display data for specific values of t/L (dashed line in the main frames), showing that the convergence to the asymptotic behavior is compatible with an $O(L^{-3/4})$ approach (dashed red lines).

to be somewhat independent of them. Further investigations are called for to classify the extension of such independence.

The above phenomenological scaling theory has been checked on the quantum Ising chain. The dynamic FSS laws for the magnetization and its susceptibility follow Eq. (5), in which the parameter μ corresponds to either $\delta = g - g_c$ or h in Eq. (1). In particular, for $\delta = h = 0$, one obtains $m(t) = 0$ by symmetry, and

$$R_\chi(t, t_m, p, L) \equiv \frac{\chi(t) - 1}{\chi(t = 0) - 1} \approx \mathcal{R}_\chi(tL^{-z}, pL^{\varepsilon}). \qquad (6)$$

Results for a system at criticality, the quantum critical point, with random local longitudinal and transverse spin measurements, are shown in Fig. 4. Data for R_χ versus tL^{-z} nicely agree with Eq. (6), and corrections to the scaling are consistent with a $L^{-3/4}$ approach, as expected (see the insets). Analogous scaling results are obtained in the small-t_m limit, and also for the magnetization at $h \neq 0$, keeping hL^{y_h} constant; these are shown in Appendix C.

We finally focus on situations far from phase transitions, for example, $g > g_c$ in quantum Ising models. In such case, the system lies in the disordered phase, where the length scale ξ of quantum correlations and the gap Δ remain finite with increasing L. The data in Fig. 5 for R_χ at fixed size L suggest that, away from criticality, the characteristic time τ_m of the measurements scales as $\tau_m \sim p^{-1}$, unlike the critical behavior, where $\tau_m \sim p^{-\kappa}$ with $\kappa = z/\varepsilon < 1$.

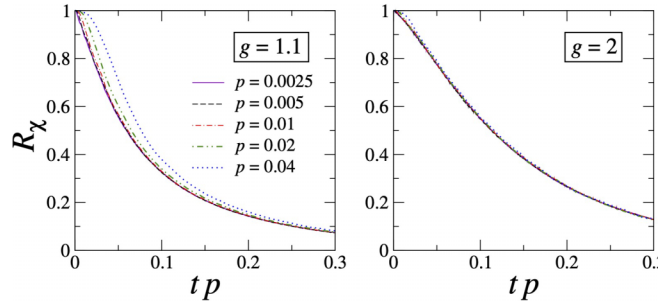

FIG. 5. R_χ for the Ising chain with $L = 10$, $h = 0$, as a function of tp. Local measurements are performed along $\sigma_x^{(3)}$, with $t_m = 0.1$ and varying p (see legend). We fix $g = 1.1$ (left) or $g = 2$ (right). The approximate collapse of the data versus tp suggests that the characteristic time τ_m scales as $\tau_m \sim p^{-1}$.

IV. SUMMARY AND CONCLUSIONS

We unveiled different regimes arising from the interplay between unitary and projective dynamics in critical systems. One of them is dominated by local random measurements, for example for any finite probability p of making the measurement. In contrast, for sufficiently small p values (decreasing as a sufficiently large power of the inverse diverging length scale ξ), the measurements are irrelevant. We conjectured these two regimes to be separated by dynamic conditions imposing suitable scaling behaviors for the characterizing parameters of the protocol, controlled by the universality class of the quantum transition. For a d-dimensional critical system, this occurs when $p \sim \xi^{-\varepsilon}$, for which we argue $\varepsilon = z + d$. This scenario is supported by numerical results for the quantum Ising chain, with measurements performed along the transverse or the longitudinal component of the local spin operator. Local measurements generally suppress quantum correlations, even in the dynamic scaling limit, with scaling laws that are qualitatively different when being far from criticality. The corresponding timescale at a quantum transition is indeed expected to behave as $\tau_m \sim p^{-\kappa}$ with $\kappa = z/\varepsilon < 1$, to be compared with the noncritical case $\tau_m \sim p^{-1}$. The smaller power κ at criticality (i.e., faster decay rate) can be explained by the fact that the relevant probability (p_r) driving the measurement process is the one to perform a local measurement within the critical volume ξ^d; therefore $p_r = p\xi^d$. The time rate thus behaves as $\tau_m \sim p_r^{-1}$, similarly to the noncritical case, where $\xi = O(1)$.

Additional checks are called for to definitely validate our scaling conjectures, such as to study protocols with Hamiltonian quenches, higher dimensions, and other quantum transitions and measurement schemes (not necessarily strictly on-site, yet sufficiently local). Moreover, arguments similar to those employed here should hold for measurements localized in restricted regions of space, and also close to first-order quantum transitions, where boundary conditions could be relevant [39,50].

Given the relatively small sizes required to reach the dynamic FSS limit (see Fig. 4), a direct experimental realization of our protocol can be reasonably considered as a near-future target for quantum simulations. Promising platforms are superconducting quantum circuits [51–53], nuclear

spins [54,55], trapped ions [56–58], and ultracold atomic systems [59–62].

ACKNOWLEDGMENTS

We thank M. Collura, A. De Luca, and A. De Pasquale for fruitful discussions. D.R. acknowledges the Italian MIUR through PRIN Project No. 2017E44HRF.

APPENDIX A: PHENOMENOLOGICAL SCALING THEORY OF THE OUT-OF-EQUILIBRIUM DYNAMICS INDUCED BY LOCAL MEASUREMENTS

We work out a phenomenological scaling theory for the out-of-equilibrium dynamics arising from random local projective measurements during the evolution of a many-body system at a quantum transition [7]. For simplicity, we assume that the quantum transition is driven by a relevant parameter μ of the Hamiltonian $H(\mu)$, whose critical value is $\mu_c = 0$. At the critical point, the low-energy unitary Hamiltonian dynamics develops long-distance correlations, characterized by a diverging length scale $\xi \sim |\mu|^{-\nu}$, where $\nu = 1/y_\mu$ and y_μ is the RG dimension of the relevant parameter.

More specifically, we consider the dynamic problem associated with the following protocol: (a) The system starts at $t = 0$ from the ground state close to the critical point, thus $|\mu| \ll 1$. (b) Random local measurements are performed every time interval t_m, with a homogeneous probability p per site. Between two measurement steps, the system evolution is driven by the unitary operator $e^{-iH(\mu)t}$. Hereafter we adopt units of $\hbar = k_B = 1$.

The out-of-equilibrium critical dynamics at continuous quantum transitions has been shown to obey homogeneous scaling laws [30–42], even in the presence of dissipation [43,44]. For example, after an instantaneous quench from $\mu_0 = 0$ to μ, a generic observable B at fixed time t after the quench is generally expected to behave as [39]

$$B(\mu, t, L) \approx b^{-y_B} \mathcal{B}(\mu b^{y_\mu}, t b^{-z}, L/b), \tag{A1}$$

where b is an arbitrary positive parameter, L is the linear size of the d-dimensional system under investigation, and $\mathcal{B}$ is a universal scaling function apart from normalizations. The exponent y_B denotes the RG dimension of the operator associated to B, while the dynamic exponent z characterizes the behavior of the energy differences of the lowest-energy states and, in particular, the ground-state gap $\Delta \sim L^{-z}$. Equation (A1) is expected to provide the asymptotic power-law behavior in the large-b limit.

We now extend the dynamic scaling arguments leading to Eq. (A1), by allowing for the dependence on the parameters t_m and p which characterize the measurement procedure of the protocol. As a working hypothesis, we assume that an asymptotic scaling behavior is achieved by appropriately rescaling t_m and p, such as in Eq. (3):

$$B(\mu, t, t_m, p, L) \approx b^{-y_B} \mathcal{B}(\mu b^{y_\mu}, t b^{-z}, t_m b^{\zeta}, p b^{\varepsilon}, L/b), \tag{A2}$$

where ζ and ε are appropriate exponents whose relevance is discussed below.

1. Dynamic finite-size scaling

It is possible to exploit the arbitrariness of the scale parameter b. For example, by setting $b = L$, we obtain the dynamic FSS equations, extending those holding for closed systems [8,39,47,49]. To achieve a nontrivial competition with the critical modes, it is reasonable to assume the scaling behaviors $t_m \sim L^z$ and $p \sim L^{-z-d}$ for the parameters t_m and p characterizing the measurement process. Comparing with Eq. (A2), this implies that

$$\zeta = -z, \quad \varepsilon = z + d. \tag{A3}$$

On the basis of these scaling arguments, from Eq. (A2) we conjecture that, keeping t_m and the arguments of the scaling function $\mathcal{B}$ fixed, the dynamic FSS law associated with the random-measurement protocol reads

$$B(\mu, t, t_m, p, L) \approx L^{-y_B} \mathcal{B}(\mu L^{y_\mu}, t L^{-z}, p L^{\varepsilon}). \tag{A4}$$

The scaling function $\mathcal{B}$ is expected to be largely universal with respect to the Hamiltonian of the system, within a given universality class, and also with respect to the details of the protocol. Of course, like any scaling function for a quantum transition, such universality is expected modulo a multiplicative overall constant and normalizations of the scaling variables. Note that in this case, the asymptotic scaling behavior does not depend on t_m and therefore it is expected to hold also in the limit $t_m \to 0$.

Alternatively, one may rescale the time interval t_m as $\tau \sim L^z$, thus keeping the ratio t_m/L^z fixed. In this case we expect the probability p to scale as the inverse volume only, i.e.,

$$B(\mu, t, t_m, p, L) \approx L^{-y_B} \mathcal{B}(\mu L^{y_\mu}, t L^{-z}, t_m L^{-z}, p L^{d}). \tag{A5}$$

Note that analogously to Eq. (A4), the FSS limit requires that $p/t_m \sim L^{-\varepsilon}$. Similar scaling *Ansätze* for more general observables, such as fixed-time correlation functions of two operators, can be straightforwardly obtained using the same assumptions and scaling arguments.

The above predictions can be extended to the more complex protocol including an initial quench of the Hamiltonian parameter from μ_0 to μ; this is achieved by adding the further dependence on $\mu_0 L^{y_\mu}$. Moreover, one may also consider an initial Gibbs state for a small temperature T, and this can be taken into account by adding further scaling variables $T L^z$.

We finally note that our scaling arguments do not apparently depend on the type of local measurement; thus they are expected to be somewhat independent of them.

2. Dynamic scaling in the thermodynamic limit

To derive a dynamic scaling theory for infinite-volume systems, we may restart from the general homogeneous power law in Eq. (A2) and set

$$b = \lambda \equiv |\mu|^{1/y_\mu}, \tag{A6}$$

where λ is the length scale of the critical modes, and consider the limit $L/\lambda \to \infty$, assuming that it is well defined (this limit corresponds to the so-called *thermodynamic* limit, which is expected to be well defined for any $\mu \neq 0$, for which λ is finite). Then, keeping again t_m fixed such that $t_m/\lambda^z \to 0$ in the $\lambda \to \infty$ limit, and using the fact that the power law

associated with p is expected to be characterized by the same exponent ε given in Eq. (A3), one obtains the dynamic scaling *Ansatz*

$$B(\mu, t, t_m, p) \approx \lambda^{-y_B} \mathcal{B}(t\lambda^{-z}, p\lambda^{\varepsilon}), \tag{A7}$$

where $\varepsilon = z + d$ is given as in Eq. (A3). Note that strictly speaking, one has two scaling functions $\mathcal{B}$, depending on the sign of μ.

APPENDIX B: DYNAMIC SCALING WITHIN THE QUANTUM ISING MODEL

The 1D quantum Ising model in a transverse field, described by the Hamiltonian in Eq. (1), is one of the simplest paradigmatic quantum many-body systems exhibiting a nontrivial zero-temperature phase diagram. As stated in Sec. II, the model undergoes a continuous quantum transition at $g = g_c = 1$ and $h = 0$, belonging to the two-dimensional Ising universality class [28].

For dynamic protocols using the quantum Ising Hamiltonian in Eq. (1), the evolution of the system can be effectively characterized by the time-dependent magnetization along the coupling direction

$$m(t) = \frac{1}{L} \sum_x \langle \sigma_x^{(3)} \rangle_t, \tag{B1a}$$

the fixed-time longitudinal correlation function

$$G(x, y, t) = \langle \sigma_x^{(3)} \sigma_y^{(3)} \rangle_t, \tag{B1b}$$

and the corresponding susceptibility

$$\chi(t) = \frac{1}{L} \sum_{x,y} G(x, y, t). \tag{B1c}$$

Here $\langle \cdot \rangle_t$ indicates the expectation value of a given observable at time t. Note that translation invariance, which also applies in finite-size systems with periodic boundary conditions, implies $G(x, y, t) \equiv G(x - y, t)$.

For the sake of presentation and without loss of generality, we fix $g = g_c$ and only vary h, so that h corresponds to the parameter μ of the above-reported scaling equations (analogous equations would hold if g were varied, with the substitution $h \to \delta$ and $y_h \to y_\delta$). The dynamic FSS laws of the observables (B1a)–(B1c), keeping t_m fixed, thus read

$$m(h, t, t_m, p, L) \approx L^{-y_m} \mathcal{M}(hL^{y_h}, tL^{-z}, pL^{\varepsilon}), \tag{B2a}$$

$$G(x, h, t, t_m, p, L) \approx L^{-2y_m} \mathcal{G}(\tfrac{x}{L}, hL^{y_h}, tL^{-z}, pL^{\varepsilon}), \tag{B2b}$$

$$\chi(h, t, t_m, p, L) \approx L^{d-2y_m} \mathcal{C}(hL^{y_h}, tL^{-z}, pL^{\varepsilon}), \tag{B2c}$$

where y_m is the RG dimension of the longitudinal spin operator $\sigma_x^{(3)}$, given by

$$y_m = \tfrac{1}{2}\big(d + z - 2 + \eta\big), \tag{B3}$$

and the power of the prefactor associated with the longitudinal spin correlation (B1b) is twice y_m ($y_m = 1/8$, in 1D). In particular, for $h = 0$ one has $m(t) = 0$ and

$$\chi(t, t_m, p, L) \approx L^{d-2y_m} \mathcal{C}(tL^{-z}, pL^{\varepsilon}). \tag{B4}$$

Corrections to scaling are generally expected to be $O(1/L)$; see for example Refs. [39,42,47]. However we note that, in the case of the susceptibility χ defined as in Eq. (B1c), $O(L^{-d+2y_m})$ corrections are also present, already at the level of the equilibrium ground-state values of χ, due to analytic contributions to the critical behavior, as explained in Ref. [47]. Therefore, in the case of the Ising chain, we expect that the leading scaling corrections to the asymptotic dynamic scaling of the evolution of χ are $O(L^{-3/4})$.

Our numerical results show that the measurement process generally tends to suppress quantum correlations; therefore $\chi(t)$ is a monotonic decreasing function. In particular, the numerics provides evidence of the fact that

$$\lim_{t\to\infty} \chi(t) = 1. \tag{B5}$$

The asymptotic value corresponds to a fully disordered state with vanishing correlations, $G(x, y, t \to \infty) = 0$ (for $x \neq y$), and where the only nonzero contributions entering the sum (B1c) are those for $x = y$, which trivially sum up to 1. To monitor the suppression of quantum correlations due to the measurement process, it is thus convenient to introduce the ratio

$$R_\chi = \frac{\chi(t) - 1}{\chi(t = 0) - 1}, \tag{B6}$$

which goes from 1 (for $t = 0$) to zero (for $t \to \infty$). In the dynamic scaling limit at the critical point, using Eq. (B4), we can immediately derive the asymptotic behavior

$$R_\chi(t, t_m, p, L) \approx \mathcal{R}_\chi(tL^{-z}, pL^{\varepsilon}). \tag{B7}$$

Note that in the dynamic scaling limit, $R_\chi \approx \chi(t)/\chi(0)$; i.e., the finite subtraction of 1 in the numerator and denominator of the definition of R_χ turns out to be irrelevant. Therefore, like for the susceptibility, the approach to the asymptotic dynamic FSS behavior (B7) is expected to be characterized by $O(L^{-3/4})$ corrections for the quantum Ising chain (see Fig. 4).

In the infinite-volume limit, at $g = g_c$, we expect to have

$$m(h, t, t_m, p) \approx \lambda^{-y_m} \mathcal{M}(t\lambda^{-z}, p\lambda^{\varepsilon}), \tag{B8a}$$

$$G(x, h, t, t_m, p) \approx \lambda^{-2y_m} \mathcal{G}(x/\lambda, t\lambda^{-z}, p\lambda^{\varepsilon}), \tag{B8b}$$

$$\chi(h, t, t_m, p) \approx \lambda^{d-2y_m} \mathcal{C}(t\lambda^{-z}, p\lambda^{\varepsilon}), \tag{B8c}$$

where $\lambda = |h|^{-1/y_h}$. Such dynamic scaling behaviors are expected to be approached asymptotically for $L \to \infty$, keeping fixed the scaling variables of the functions $\mathcal{M}$ and $\mathcal{C}$.

As already noted above, the dynamic scaling arguments that we have outlined do not apparently depend on the type of local measurement. In particular, in the case of the quantum Ising model, they should apply to protocols based on both $\sigma_x^{(1)}$ or $\sigma_x^{(3)}$ local measurements.

The timescale τ_m of the suppression of the quantum correlations may be estimated from the halving time of $R_\chi(t)$. Its power-law scaling behavior in terms of the probability p can be easily derived in the dynamic scaling limit, by noting that $p \sim \xi^{-\varepsilon}$ and $t \sim \xi^z$, where ξ is the length scale of the critical modes (that is $\xi \sim L$ at the critical point and $\xi \sim \lambda$ around it). Therefore, the dynamic scaling predicts that the timescale τ_m associated with the suppression of the quantum correlations

behaves as

$$\tau_m \sim p^{-\kappa}, \qquad \kappa = \frac{z}{\varepsilon} = \frac{z}{z+d}. \tag{B9}$$

Note that $\kappa < 1$; thus the time rate in terms of p turns out to be accelerated with respect the noncritical behavior $\tau_m \sim p^{-1}$ which has been obtained numerically (see Fig. 5). As stated in Sec. III, this apparently counterintuitive behavior can be explained by the nontrivial fact that the relevant probability p_r, which drives the measurement process, is the probability to perform a local measurement within the critical volume ξ^d.

APPENDIX C: DETAILS ON THE NUMERICAL COMPUTATIONS

To check our phenomenological dynamic scaling theory discussed before, we have performed some numerical simulations on the 1D quantum Ising chain (1), based on exact diagonalization (ED). We are interested in the random-measurement protocol starting from the ground state of a system of size L (with periodic boundary conditions) for the Hamiltonian parameter h and with $g = g_c = 1$, which has been obtained by means of a Lanczos technique. The evolution is essentially driven by the random measurements, which are performed at every time interval t_m. We have considered either local longitudinal $[\sigma_x^{(3)}]$ or transverse $[\sigma_x^{(1)}]$ measurements, occurring with a probability p per site. For the dynamics between consecutive measurements, we employed a fourth-order Suzuki-Trotter decomposition of the unitary-evolution operator, with time step $dt = 5 \times 10^{-3}$ (this value ensures convergence on the scale of all figures, over the largest reached system size).

Results at any time t have been averaged over $N_{\rm avg}$ trajectories, with $N_{\rm avg} = 2 \times 10^4$ up to $L = 14$ sites, and $N_{\rm avg} = 2 \times 10^3$ for $L > 14$ The need of averaging over many different trajectories, together with the fact that the numerical results shown in this paper are nicely consistent with the dynamic FSS theory, prevented us from studying systems with more than $L = 18$ sites, although larger sizes would be easily addressable for a single trajectory or a few ones. Also note that we preferred to use conventional (and fully controllable) ED techniques over DMRG-based algorithms [5,63], since with those latter methods it is more complicated to guarantee the required accuracy in order to carefully test our phenomenological scaling theory. Nonetheless, there are no conceptual limitations in using DMRG for analyzing the measurement-induced dynamics of quantum lattice models with finite degrees of freedom [23]. In summary, ED techniques are more controllable, but suffer from severe limitations in the reachable system sizes; DMRG allows us to study larger systems, although it requires more care in the choice of the bond-link dimension for the study of dynamical problems.

In Sec. III, we showed results only for the susceptibility ratio R_χ (Fig. 4). Here we provide some additional data, both for the magnetization (B1a) and for the susceptibility (B1c), in which we kept $g = 1$ and varied the longitudinal field h (note that the quantum Ising chain with $h \neq 0$ is not integrable).

Figure 6 displays the numerical outcomes for the susceptibility at the Ising critical point ($g = 1$, $h = 0$), for random local measurements taken along the longitudinal or the transverse direction. Note that the results presented in this figure are the same as those reported in Fig. 4, but for the rescaled susceptibility $\chi L^{-3/4}$ [instead of the ratio R_χ in Eq. (B6)]. Similarly to the case for the susceptibility ratio, we observe a nice agreement with the predicted scaling behavior in Eq. (B2c). Moreover, corrections to the scaling are consistent with a $L^{-3/4}$ behavior, as expected (see the two insets).

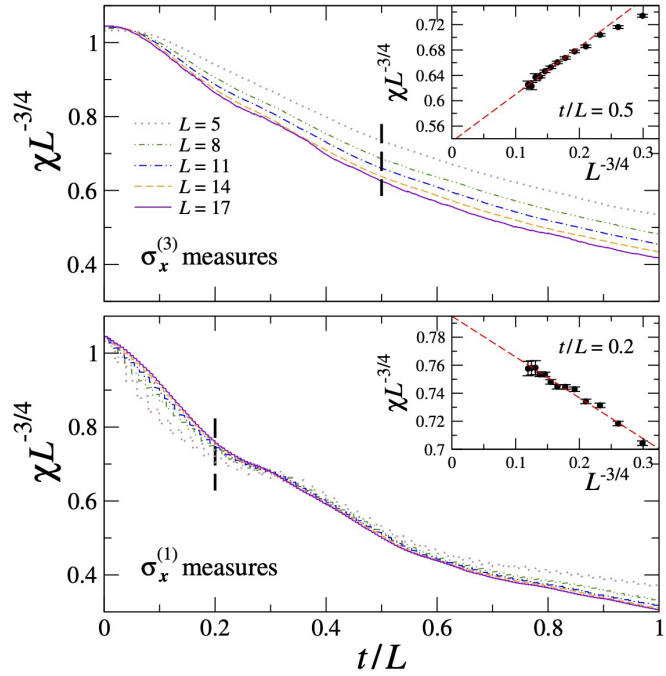

FIG. 6. Rescaled susceptibility $\chi L^{-3/4}$ at criticality (g=1, h=0), as a function of the rescaled time t/L, for the quantum Ising chain with different system sizes L (see legend). The upper panel refers to random measures along the longitudinal direction $[\sigma_x^{(3)}]$, while the lower panel refers to random measures along the transverse direction $[\sigma_x^{(1)}]$. Measurements are characterized by $t_m = 0.1$, $p = 1/L^2$ as predicted by Eq. (A3). The two insets display the same data as the main panels for a specific cut in the rescaled time ($t/L = 0.5$ for the upper frame, $t/L = 0.2$ for the lower frame) versus $L^{-3/4}$. The approach to the asymptotic value is consistent with the expected $O(L^{-3/4})$ corrections. Dashed red lines denote $1/L^{3/4}$ fits to numerical data (black circles) and have been obtained by discarding points for the smaller available sizes. Here and in the next figures, data have been averaged over a number of $N_{\rm avg} = 2 \times 10^3$ (for $L \leqslant 14$) and $N_{\rm avg} = 2 \times 10^3$ (for $L \geqslant 15$) trajectories.

Results for the magnetization $m(t)$ are reported in Fig. 7. In that case, we considered $g = 1$ and a nonzero longitudinal field h, since the latter is essential in order to start from an initially magnetized state [$m(0) \neq 0$]. After a suitable rescaling of all the relevant parameters, the various curves approach an asymptotic scaling behavior, as indicated in Eq. (B2a). Notice that we also rescaled the field h so to keep the scaling variable $hL^{15/8}$ constant. The approach to the scaling is governed by corrections whose leading order appear to be consistent with a L^{-1} behavior, as witnessed by the two insets.

All the numerical data presented in this paper correspond to fixing the time interval between two consecutive measurements equal to $t_m = 0.1$. We checked that analogous scaling results can be obtained for arbitrary values of t_m. In particular,

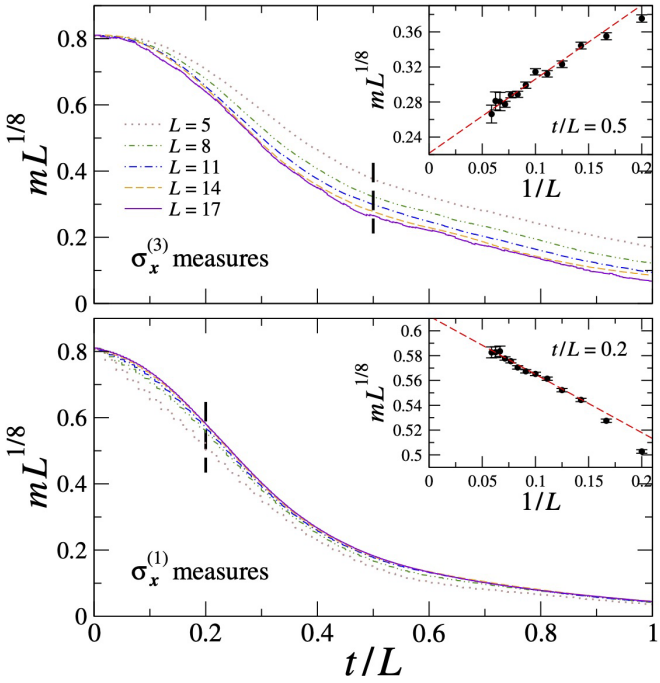

FIG. 7. Same as in Fig. 6, but for the rescaled magnetization $mL^{1/8}$ vs the rescaled time t/L. The initial state here is the ground state of the quantum Ising ring with $g = 1$ and rescaled longitudinal field $hL^{15/8} = 1$, which has a finite magnetization. The two insets display the same data as the main panels for a specific cut in the rescaled time, versus $1/L$. The approach to the asymptotic FSS behavior, for finite L, appears to be consistent with the expected $O(1/L)$ trend (dashed red lines).

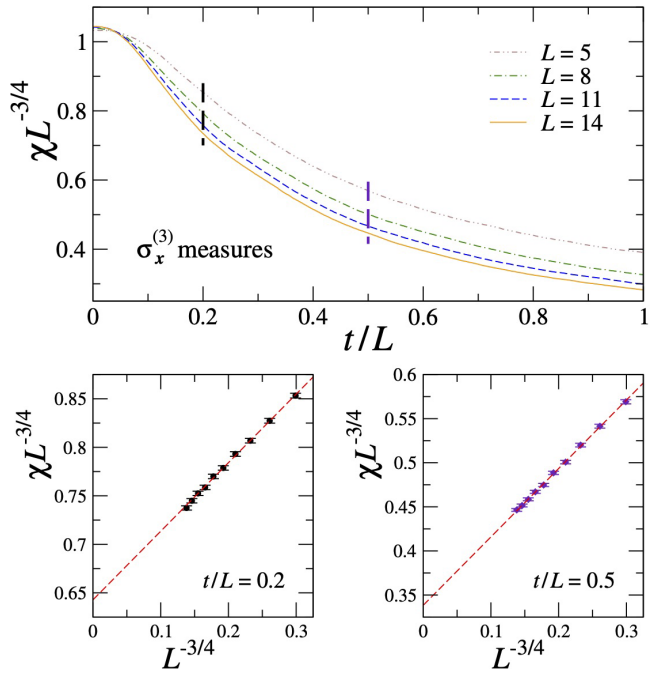

FIG. 8. Same as in Fig. 6, but for random local measurements along the longitudinal direction in the continuous-time limit $t_m \to 0$ and with $p = 0.1/L^2$. The lower panels display the same data as the main panel, for two specific values of rescaled time (left: $t/L = 0.2$; right: $t/L = 0.5$) versus $L^{-3/4}$. The approach to the asymptotic value is consistent with the expected $L^{-3/4}$ corrections (dashed red lines).

in Fig. 8 we considered the limit $t_m \to 0$. More precisely, random local measurements have been performed at every Trotter time step, so that $t_m = 0.005$. The upper panel displays results for the rescaled susceptibility $\chi L^{-3/4}$ as a function of the rescaled time t/L, keeping $g = 1$ and $h = 0$, for measurements performed along the longitudinal direction $[\sigma_x^{(3)}]$. The lower panels highlight that corrections to the scaling are $O(L^{-3/4})$, as expected. Here the compatibility with a $L^{-3/4}$ behavior (dashed red lines) is excellent already at very small system sizes, contrary to the case of larger t_m values: compare with the insets of Fig. 6, where deviations from the expected trend emerge at smaller L. This hints at the fact that other subleading terms, that may enter the scaling corrections at finite L, may get suppressed for $t_m \to 0$, such as those which are $O(t_m/L^z)$.

Finally we observe that the same scaling functions ($\mathcal{M}$, $\mathcal{G}$, $\mathcal{C}$, ...) are expected to hold for vanishing t_m, so that the asymptotic curves for the magnetization and the susceptibility at $L \to \infty$ should coincide with those at finite t_m, after a proper rescaling of all the relevant parameters in the dynamic protocol.

APPENDIX D: ONE-SPIN MODEL SUBJECT TO PERIODIC MEASUREMENTS

Here we discuss the dynamics of a single spin-1/2 system in a magnetic field, subject to periodic measurements along a given axis, for which it is possible to derive an analytic solution. We consider the following Hamiltonian model:

$$H_1 = -g\sigma^{(1)} - h\sigma^{(3)}, \tag{D1}$$

where g and h denote the intensity of an applied external magnetic field along two orthogonal directions. Without loss of generality, we fix $g = 1$. We now suppose initializing the system in its ground state, associated with the parameter h at $t = 0$. Then we perform a sequence of repeated measurements of the operator $\sigma^{(3)}$ at every time interval t_m (the choice of the measurement axis is arbitrary).

The dynamics arising from this protocol can be described in terms of the system's density matrix ρ. The starting ($t = 0$) state is a pure state, given by

$$\rho_0 \equiv \rho(t = 0) = |0_h\rangle\langle 0_h|, \tag{D2}$$

where

$$E_0 = -\sqrt{1 + h^2}, \tag{D3}$$

$$|0_h\rangle = \mathcal{N}[(-h - \sqrt{1 + h^2})|+\rangle + |-\rangle], \tag{D4}$$

and $|\pm\rangle$ are the eigenstates of $\sigma^{(3)}$, while $\mathcal{N}$ is the normalization to obtain $\langle 0_h|0_h\rangle = 1$. Then, defining the density matrix after n measurements, at time $t = nt_m$, as

$$\rho_n \equiv \rho(t = nt_m), \tag{D5}$$

the subsequent dynamics can be described as a series of two-step operations:

(i) A unitary time evolution for a time t_m,

$$\tilde{\rho}_{n+1} = e^{-iH_1 t_m} \rho_n e^{iH_1 t_m}. \tag{D6a}$$

(ii) The measurement of $\sigma^{(3)}$,

$$\rho_{n+1} = \mathrm{Tr}(\tilde{\rho}_{n+1}P_+)P_+ + \mathrm{Tr}(\tilde{\rho}_{n+1}P_-)P_-, \tag{D6b}$$

where $P_\pm$ are the projectors onto the eigenstates $|\pm\rangle$ of $\sigma^{(3)}$. Simple manipulations thus lead to

$$\rho_{n+1} = \tfrac{1}{2}I + W_{n+1}\sigma^{(3)}, \qquad W_{n+1} = \tilde{\rho}^{11}_{n+1} - \tfrac{1}{2}, \tag{D6c}$$

where W quantifies the deviation from the trivial completely unpolarized density matrix $\rho_u = I/2$. Given the initial condition (D2), one finds

$$W_1 = \frac{h(\sqrt{1+h^2}+h)}{2(1+h^2+h\sqrt{1+h^2})}. \tag{D7}$$

Straightforward computations allow one to obtain

$$W_{n+1} = f\,W_n, \qquad f = 1 - \frac{2[\sin(t_m\sqrt{1+h^2})]^2}{1+h^2}. \tag{D8}$$

In particular, for $h = 1$, one gets $W_1 = (1+\sqrt{2})/(4+2\sqrt{2}) \approx 0.35355$ and $f = 1 - \sin^2(\sqrt{2}t_m)$. Note that the factor f is bounded; indeed,

$$|f| \leqslant 1. \tag{D9}$$

Moreover, for arbitrary values of h and t_m, one strictly finds $|f| < 1$. Indeed $f = -1$ for $h = 0$ only, while $f = 1$ for the specific values $t_m = m\pi/\sqrt{1+k^2}$, with integer m.

Equation (D8) implies

$$W_n = W_1 f^{n-1}. \tag{D10}$$

Therefore, by monitoring the expectation value of $\sigma^{(3)}$, one eventually gets

$$\langle\sigma^{(3)}\rangle_{t=nt_m} = \mathrm{Tr}[\sigma^{(3)}\rho_n] = 2W_n = 2W_1 f^{n-1}. \tag{D11}$$

Since in general $|f| < 1$, this shows that for any h the dynamic protocol tends to produce disorder in the spin model, leading to a completely unpolarized density matrix.

For the specific case of sufficiently small $t_m \ll 1$, one finds

$$f = 1 - 2t_m^2 + O(t_m^4), \tag{D12}$$

and thus

$$W_n \sim (1-2t_m^2)^n \approx e^{-2t_m^2 n}. \tag{D13}$$

Therefore, the dependence on h disappears in the leading $O(t_m^2)$ term. Finally, we note that in the limit $t_m \to 0$, the quantum Zeno effect [11,12] can be recovered; indeed one simply has $f \to 1$ and $W_n \to 1$.

[1] M. Müller, S. Diehl, G. Pupillo, and P. Zoller, Engineered open systems and quantum simulations with atoms and ions, Adv. At. Mol. Opt. Phys. **61**, 1 (2012).

[2] A. A. Houck, H. E. Türeci, and J. Koch, On-chip quantum simulation with superconducting circuits, Nat. Phys. **8**, 292 (2012).

[3] H. Ritsch, P. Domokos, F. Brennecke, and T. Esslinger, Cold atoms in cavity-generated dynamical optical potentials, Rev. Mod. Phys. **85**, 553 (2013).

[4] I. Carusotto and C. Ciuti, Quantum fluids of light, Rev. Mod. Phys. **85**, 299 (2013).

[5] A. J. Daley, Quantum trajectories and open many-body quantum systems, Adv. Phys. **63**, 77 (2014).

[6] L. M. Sieberer, M. Buchhold, and S. Diehl, Keldysh field theory for driven open quantum systems, Rep. Prog. Phys. **79**, 096001 (2016).

[7] S. Sachdev, *Quantum Phase Transitions* (Cambridge University Press, 1999).

[8] S. L. Sondhi, S. M. Girvin, J. P. Carini, and D. Shahar, Continuous quantum phase transitions, Rev. Mod. Phys. **69**, 315 (1997).

[9] W. H. Zurek, Decoherence, einselection, and the quantum origins of the classical, Rev. Mod. Phys. **75**, 715 (2003).

[10] J. von Neumann, *Mathematical Foundations of Quantum Mechanics: New Edition*, edited by N. A. Wheeler (Princeton University Press, 2018).

[11] B. Misra and E. C. G. Sudarshan, The Zeno's paradox in quantum theory, J. Math. Phys. **18**, 756 (1977).

[12] P. Facchi and S. Pascazio, Quantum Zeno dynamics: Mathematical and physical aspects, J. Phys. A: Math. Theor. **41**, 493001 (2008).

[13] Y. Li, X. Chen, and M. P. A. Fisher, Quantum Zeno effect and the many-body entanglement transition, Phys. Rev. B **98**, 205136 (2018).

[14] A. Chan, R. M. Nandkishore, M. Pretko, and G. Smith, Unitary-projective entanglement dynamics, Phys. Rev. B **99**, 224307 (2019).

[15] B. Skinner, J. Ruhman, and A. Nahum, Measurement-Induced Phase Transitions in the Dynamics of Entanglement, Phys. Rev. X **9**, 031009 (2019).

[16] Y. Li, X. Chen, and M. P. A. Fisher, Measurement-driven entanglement transition in hybrid quantum circuits, Phys. Rev. B **100**, 134306 (2019).

[17] M. Szyniszewski, A. Romito, and H. Schomerus, Entanglement transition from variable-strength weak measurements, Phys. Rev. B **100**, 064204 (2019).

[18] M. J. Gullans and D. A. Huse, Dynamical purification phase transitions induced by quantum measurements, arXiv:1905.05195.

[19] Y. Bao, S. Choi, and E. Altman, Theory of the phase transition in random unitary circuits with measurements, Phys. Rev. B **101**, 104301 (2020).

[20] C.-M. Jian, Y.-Z. You, R. Vasseur, and A. W. W. Ludwig, Measurement-induced criticality in random quantum circuits, Phys. Rev. B **101**, 104302 (2020).

[21] M. J. Gullans and D. A. Huse, Scalable probes of measurement-induced criticality, arXiv:1910.00020.

[22] A. Zabalo, M. J. Gullans, J. H. Wilson, S. Gopalakrishnan, D. A. Huse, and J. H. Pixley, Critical properties of the measurement-induced transition in random quantum circuits, Phys. Rev. B **101**, 060301(R) (2020).

[23] Q. Tang and W. Zhu, Measurement-induced phase transition: A case study in the non-integrable model by density-matrix renormalization group calculations, Phys. Rev. Research **2**, 013022 (2020).

[24] S. Goto and I. Danshita, Measurement-induced transitions of the entanglement scaling law in ultracold gases with controllable dissipation, arXiv:2001.03400.

[25] S. Dhar and S. Dasgupta, Measurement-induced phase transition in a quantum spin system, Phys. Rev. A **93**, 050103(R) (2016).

[26] S. Roy, J. T. Chalker, I. V. Gornyi, and Y. Gefen, Measurement-induced steering of quantum systems, arXiv:1912.04292.

[27] X. Cao, A. Tilloy, and A. De Luca, Entanglement in a fermion chain under continuous monitoring, SciPost Phys. **7**, 024 (2019).

[28] For the quantum Ising chain, the critical point is located at $g_c = 1$, $h = 0$. The RG dimensions of the control parameters δ and h are $y_\delta = 1$ and $y_h = 15/8$. The exponent describing the critical two-point function is $\eta = 1/4$, which determines the RG dimension of the longitudinal spin operator $y_m = (d + z - 2 + \eta)/2$ and the power law $\chi \sim \xi^{d-2y_m}$ [47]. For 2D models, the critical exponents are not known exactly, but there are very accurate estimates [29]: $y_\delta = 1/\nu$ with $\nu = 0.629971(4)$ and $y_h = (5 - \eta)/2$ with $\eta = 0.036298(2)$. For 3D systems, they assume mean-field values, $y_\delta = 2$ and $y_h = 3$, neglecting logarithmic corrections.

[29] A. Pelissetto and E. Vicari, Critical phenomena and renormalization-group theory, Phys. Rep. **368**, 549 (2002); F. Kos, D. Poland, D. Simmons-Duffin, and A. Vichi, Precision islands in the Ising and O(N) models, J. High Energy Phys. 08 (2016) 036.

[30] W. H. Zurek, U. Dorner, and P. Zoller, Dynamics of a Quantum Phase Transition, Phys. Rev. Lett. **95**, 105701 (2005).

[31] J. Dziarmaga, Dynamics of a Quantum Phase Transition: Exact Solution of the Quantum Ising Model, Phys. Rev. Lett. **95**, 245701 (2005).

[32] S. Gong, F. Zhong, X. Huang, and S. Fan, Finite-time scaling via linear driving, New J. Phys. **12**, 043036 (2010).

[33] A. Polkovnikov, K. Sengupta, A. Silva, and M. Vengalattore, Colloquium: Nonequilibrium dynamics of closed interacting quantum systems, Rev. Mod. Phys. **83**, 863 (2011).

[34] A. Chandran, A. Erez, S. S. Gubser, and S. L. Sondhi, Kibble-Zurek problem: Universality and the scaling limit, Phys. Rev. B **86**, 064304 (2012).

[35] S. Ulm, J. Roßnagel, G. Jacob, C. Degünther, S. T. Dawkins, U. G. Poschinger, R. Nigmatullin, A. Retzker, M. B. Plenio, F. Schmidt-Kaler, and K. Singer, Observation of the Kibble-Zurek scaling law for defect formation in ion crystals, Nat. Commun. **4**, 2290 (2013).

[36] K. Pyka, J. Keller, H. L. Partner, R. Nigmatullin, T. Burgermeister, D. M. Meier, K. Kuhlmann, A. Retzker, M. B. Plenio, W. H. Zurek, A. del Campo, and T. E. Mehlstäubler, Topological defect formation and spontaneous symmetry breaking in ion Coulomb crystals, Nat. Commun. **4**, 2291 (2013).

[37] G. Biroli, in *Strongly Interacting Quantum Systems out of Equilibrium*, edited by T. Giamarchi, A. J. Millis, O. Parcollet, H. Saleur, and L. F. Cugliandolo, Lecture Notes of the Les Houches Summer School: Vol. 99 (Oxford University Press, Oxford, 2016).

[38] P. Calabrese and J. Cardy, Quantum quenches in $1 + 1$ dimensional conformal field theories, J. Stat. Mech. (2016) 064003.

[39] A. Pelissetto, D. Rossini, and E. Vicari, Dynamic finite-size scaling after a quench at quantum transitions, Phys. Rev. E **97**, 052148 (2018).

[40] A. Pelissetto, D. Rossini, and E. Vicari, Out-of-equilibrium dynamics driven by localized time-dependent perturbations at quantum phase transitions, Phys. Rev. B **97**, 094414 (2018).

[41] D. Nigro, D. Rossini, and E. Vicari, Scaling properties of work fluctuations after quenches near quantum transitions, J. Stat. Mech. (2019) 023104.

[42] D. Rossini and E. Vicari, Scaling of decoherence and energy flow in interacting quantum spin systems, Phys. Rev. A **99**, 052113 (2019).

[43] S. Yin, P. Mai, and F. Zhong, Nonequilibrium quantum criticality in open systems: The dissipation rate as an additional indispensable scaling variable, Phys. Rev. B **89**, 094108 (2014); S. Yin, C.-Y. Lo, and P. Chen, Scaling behavior of quantum critical relaxation dynamics of a system in a heat bath, *ibid.* **93**, 184301 (2016).

[44] D. Nigro, D. Rossini, and E. Vicari, Competing coherent and dissipative dynamics close to quantum criticality, Phys. Rev. A **100**, 052108 (2019); D. Rossini and E. Vicari, Scaling behavior of the stationary states arising from dissipation at continuous quantum transitions, Phys. Rev. B **100**, 174303 (2019).

[45] M. N. Barber, in *Phase Transitions and Critical Phenomena*, edited by C. Domb and J. L. Lebowitz (Academic Press, New York, 1983).

[46] V. Privman (editor), *Finite Size Scaling and Numerical Simulation of Statistical Systems* (World Scientific, Singapore, 1990).

[47] M. Campostrini, A. Pelissetto, and E. Vicari, Finite-size scaling at quantum transitions, Phys. Rev. B **89**, 094516 (2014).

[48] Note that, strictly speaking, one has two scaling functions $\mathcal{B}$, depending on the sign of μ.

[49] M. Campostrini, J. Nespolo, A. Pelissetto, and E. Vicari, Finite-Size Scaling at First-Order Quantum Transitions, Phys. Rev. Lett. **113**, 070402 (2014).

[50] A. Pelissetto, D. Rossini, and E. Vicari, Finite-size scaling at first-order quantum transitions when boundary conditions favor one of the two phases, Phys. Rev. E **98**, 032124 (2018).

[51] R. Barends, L. Lamata, J. Kelly, L. García-Álvarez, A. G. Fowler, A. Megrant, E. Jeffrey, T. C. White, D. Sank, J. Y. Mutus *et al.*, Digital quantum simulation of fermionic models with a superconducting circuit, Nat. Commun. **6**, 7654 (2015).

[52] R. Harris, Y. Sato, A. J. Berkley, M. Reis, F. Altomare, M. H. Amin, K. Boothby, P. Bunyk, C. Deng, C. Enderud *et al.*, Phase transitions in a programmable quantum spin glass simulator, Science **361**, 162 (2018).

[53] Z. K. Minev, S. O. Mundhada, S. Shankar, P. Reinhold, R. Gutiérrez-Jáuregui, R. J. Schoelkopf, M. Mirrahimi, H. J. Carmichael, and M. H. Devoret, To catch and reverse a quantum jump mid-flight, Nature (London) **570**, 200 (2019).

[54] L. Jiang, J. S. Hodges, J. R. Maze, P. Maurer, J. M. Taylor, D. G. Cory, P. R. Hemmer, R. L. Walsworth, A. Yacoby, A. S. Zibrov, and M. D. Lukin, Repetitive readout of a single electronic spin via quantum logic with nuclear spin ancillae, Science **326**, 267 (2009).

[55] N. Kalb, J. Cramer, D. J. Twitchen, M. Markham, R. Hanson, and T. H. Taminiau, Experimental creation of quantum Zeno

subspaces by repeated multi-spin projections in diamond, Nat. Commun. **7**, 13111 (2016).

[56] J. Zhang, G. Pagano, P. W. Hess, A. Kyprianidis, P. Becker, H. Kaplan, A. V. Gorshkov, Z.-X. Gong, and C. Monroe, Observation of a many-body dynamical phase transition with a 53-qubit quantum simulator, Nature (London) **551**, 601 (2017).

[57] V. Negnevitsky, M. Marinelli, K. K. Mehta, H. Y. Lo, C. Flühmann, and J. P. Home, Repeated multi-qubit reaout and feedback with a mixed-species trapped-ion register, Nature (London) **563**, 527 (2018).

[58] T. Brydges, A. Elben, P. Jurcevic, B. Vermersch, C. Maier, B. P. Lanyon, P. Zoller, R. Blatt, and C. F. Roos, Probing Rényi entanglement entropy via randomized measurements, Science **364**, 260 (2019).

[59] W. S. Bakr, J. I. Gillen, A. Peng, S. Fölling, and M. Greiner, A quantum gas microscope for detecting single atoms in a Hubbard-regime optical lattice, Nature (London) **462**, 74 (2009).

[60] J. F. Sherson, C. Weitenberg, M. Endres, M. Cheneau, I. Bloch, and S. Kuhr, Single-atom-resolved fluorescence imaging of an atomic Mott insulator, Nature (London) **467**, 68 (2010).

[61] Y. S. Patil, S. Chakram, and M. Vengalattore, Measurement-Induced Localization of an Ultracold Lattice Gas, Phys. Rev. Lett. **115**, 140402 (2015).

[62] H. Bernien, S. Schwartz, A. Keesling, H. Levine, A. Omran, H. Pichler, S. Choi, A. S. Zibrov, M. Endres, M. Greiner, V. Vuletić, and M. D. Lukin, Probing many-body dynamics on a 51-atom quantum simulator, Nature (London) **551**, 579 (2017).

[63] U. Schollwöck, The density-matrix renormalization group in the age of matrix product states, Ann. Phys. **326**, 96 (2011).